ARTHUR D. LITTLE, INC.

REPORT NO.
63270-03-01
JANUARY 1962

ON THE IMPACT OF PELLETS WITH THIN PLATES
THEORETICAL CONSIDERATIONS - PART I

BY GERALD V. BULL

LIQUID PROPELLANT
LOSSES DURING
SPACE FLIGHT

PREPARED FOR
THE NATIONAL AERONAUTICS
AND SPACE ADMINISTRATION
CONTRACT NO. NAS5-664

ON THE IMPACT OF PELLETS WITH THIN PLATES

THEORETICAL CONSIDERATIONS - PART 1

By

G. V. Bull
Department of Mechanical Engineering
McGill University
Montreal, Quebec

Technical Report

to

The National Aeronautics and Space Administration
Contract No. NAS 5-664

January 1962

Report 63270-03-01

Arthur D. Little, Inc.

FOREWORD

This report is the first of a series dealing with a theoretical study of the phenomenology of bumper protection from meteoric attack. It was prepared by Dr. G. V. Bull of McGill University, Montreal, Quebec, serving as a consultant to Arthur D. Little, Inc., in connection with NASA Contract No. NAS 5-664.

Dr. Bull is responsible for the approach to the problem and the draft of this report. It is inevitable that various aspects will emerge in altered emphasis subsequent to technical discussion with others. In arranging for the issuance of this report from Arthur D. Little, Inc., it seemed appropriate that one should attempt to update this work so as to reflect those considerations which emerged from technical discussions among Dr. Bull, Dr. Sydney Goldstein of Harvard University, and the writer. The report as prepared by Dr. Bull is reproduced with but minor alterations; the various features of our discussions which it appeared appropriate to record are presented as notes in this foreword. In the interest of brevity the various definitions of symbols, etc., have not been restated in the foreword. For this reason it is suggested that one read the main text and refer to these notes where such references are suggested in the text. Supplemental passages added to the body of the main text in the course of preparation for its issuance as an Arthur D. Little, Inc., report appear in double parentheses.

Note 1: Most of the materials of interest will probably exhibit a polytropic constant in excess of 2. In this case the expansion occasioned by the rarefaction wave will be somewhat constrained by the bumper since the head of the rarefaction wave will not emerge behind the bumper plate (this is discussed in the text). Attention must also be given to the possibility that radial decompression of the pellet may occur in front of the bumper plate. This circumstance would require that

$$\left[\frac{\gamma_P + 1}{\gamma_B + 1} \cdot \frac{\rho_{P_o}}{\rho_{B_o}}\right]^{\frac{1}{2}} < \frac{1}{2}(\gamma_P - 1)$$

(as is readily shown on combining equations 14, 15, and 16 of the text). Such a circumstance might well be important if $\rho_{P_o}/\rho_{B_o} \ll 1$, as current meteoric evidence would suggest.

Note 2: Chronologically Section VII was completed prior to a substantial reappraisal of Section VI. As a consequence, the model on which the expansion core is calculated is appropriate only for $\gamma_B < 2$. Values for $\gamma_B > 2$ are shown as dashes, and one would expect the core angle to be overestimated by this process. The assumption that the appropriate γ for the expansion process is the same as that for the compressive phase might be questioned; but such refinements must await subsequent study. R. H. J.

ABSTRACT

This note outlines the results of a short theoretical investigation into the impact of pellets with thin plates at very high velocities. In order to render the problem tractable to analysis, a model has been assumed which allows use of essentially one-dimensional theory to predict both the impact shock-induced conditions and the subsequent expansion flow, although the latter state has been treated subsequently as a general axisymmetric three dimensional flow. The problem has been considered in three phases.

The first phase is the shock-induced impact states, which for thin bumper plates permits one-dimensional theory to be reasonably applicable. Based on the concept of the strong shock wave, it is seen that the initial impact-induced states may be expressed readily in terms of impact velocities, initial density ratios, and the polytropic gas exponent in the shocked states.

The second phase as discussed in this note results from the extremely high temperatures generated on impact. The resultant radiative loss mechanisms result in considerable reduction in the thermodynamic states from which expansion occurs. Detailed treatment of this phase will appear in subsequent notes.

The third phase, the break up of the pellet into an expanding particle cloud, has been approached in this note from the restricted point of view of one-dimensional shock and rarefaction waves interacting with a cylindrical rarefaction. This non-stationary wave system tends to accelerate the outer-material, essentially redistributing the initial kinetic energy of the pellet. Only brief consideration into the boundaries of this flow has been made in the present note. Subsequent detailed treatment of the expanding flow phase will be presented in the near future.*

*See Foreword, Note 1

ACKNOWLEDGEMENTS

The investigation described in this note was undertaken for Arthur D. Little, Inc., in support of their program for NASA. The author is indebted particularly to Dr. R. H. Johnston of Arthur D. Little, Inc., and Professor Sydney Goldstein of Harvard University for review and clarification of the work and also to Drs. N. Wiederhorn and R. Davis, Messrs. D. Lull and J. Schad of Arthur D. Little, Inc., for valuable discussions and criticisms.

The author thanks Mrs. F. M. Wiegand for preparing the typed draft from his illegible manuscript and Mr. W. H. Friend for checking the algebra and preparing figures.

TABLE OF CONTENTS

I. INTRODUCTION

Experimentally, it has been observed that the impact of small bodies with thin plates at hypervelocity speeds results in the complete disintegration of the pellet after passage through the plate. An expanding cloud of particles is obtained, the shape of this cloud being extremely sensitive to the geometry of the impact as illustrated in Figures 1 and 2 where an end-on impact of a cylindrical pellet results in a more or less circular cross section of pellet spray while the same model colliding at approximately 45° results in the mushroom-type cross section shown in Figure 2. The nature of the particle cloud is among other things, a function of impact velocity; at low enough velocities the pellet will be fragmented with some pulverization, whereas at somewhat higher velocities, complete pulverization may occur, and finally at extremely high velocities, complete vaporization of the pellet and displaced bumper material may be expected. The little experimental evidence available (all at relatively low velocity) tends to indicate that the spray cross section is not markedly dependent upon the impact velocity.

The impact of small pellets into essentially semi-infinite targets has been the subject of study for many years; the extreme complexity of the theoretical problem has tended towards reliance on a general semi-empirical approach (References 1,2). The theoretical approaches have been based upon a fluid model, since interest in general hinges around the case when shock pressures are at least an order of magnitude greater than yield stresses. Bjork (Reference 3) has numerically solved the hydrodynamic equations to determine crater volume dependence on impact velocity. Stanyukovich (Reference 4), in considering the impact of large meteors on planets having no atmospheres, has noted the strong similarity to explosions providing the collision kinetic energy is greater than the energy density of the crystal lattice. Even when the collision energy is less than required for vaporization, he has noted that pulverization can occur, resulting in a quasi-fluid flow. The vaporization energy for most materials (sand, clay, granite, aluminum, steel, etc.) is of the order of 10^{10} to 10^{12} ergs per gram. For velocities in excess of 10 km per second, vaporization would occur and the conditions behind the impact shocks are similar to those behind explosive shocks.

In any model, the displacement phenomena are initiated by shocks generated at the instant of impact; these shocks are propagated through the collided and colliding bodies. In a series of experimental studies on the equation of state conducted at the Los Alamos Scientific Laboratory, Walsh et al (References 5,6,7) used a large plane-wave explosive accelerator to launch a 0.22 cm thick steel or nickel driver plate against desired specimens in the 3 to 5 km/sec velocity range. The subsequent shock wave and free-surface velocity was measured, and from the mechanical conservation conditions, pressure and density in the shocked state were determined. In these studies, shock pressures of up to two megabars were determined. While this is below the pressures experienced in meteor impact, it does

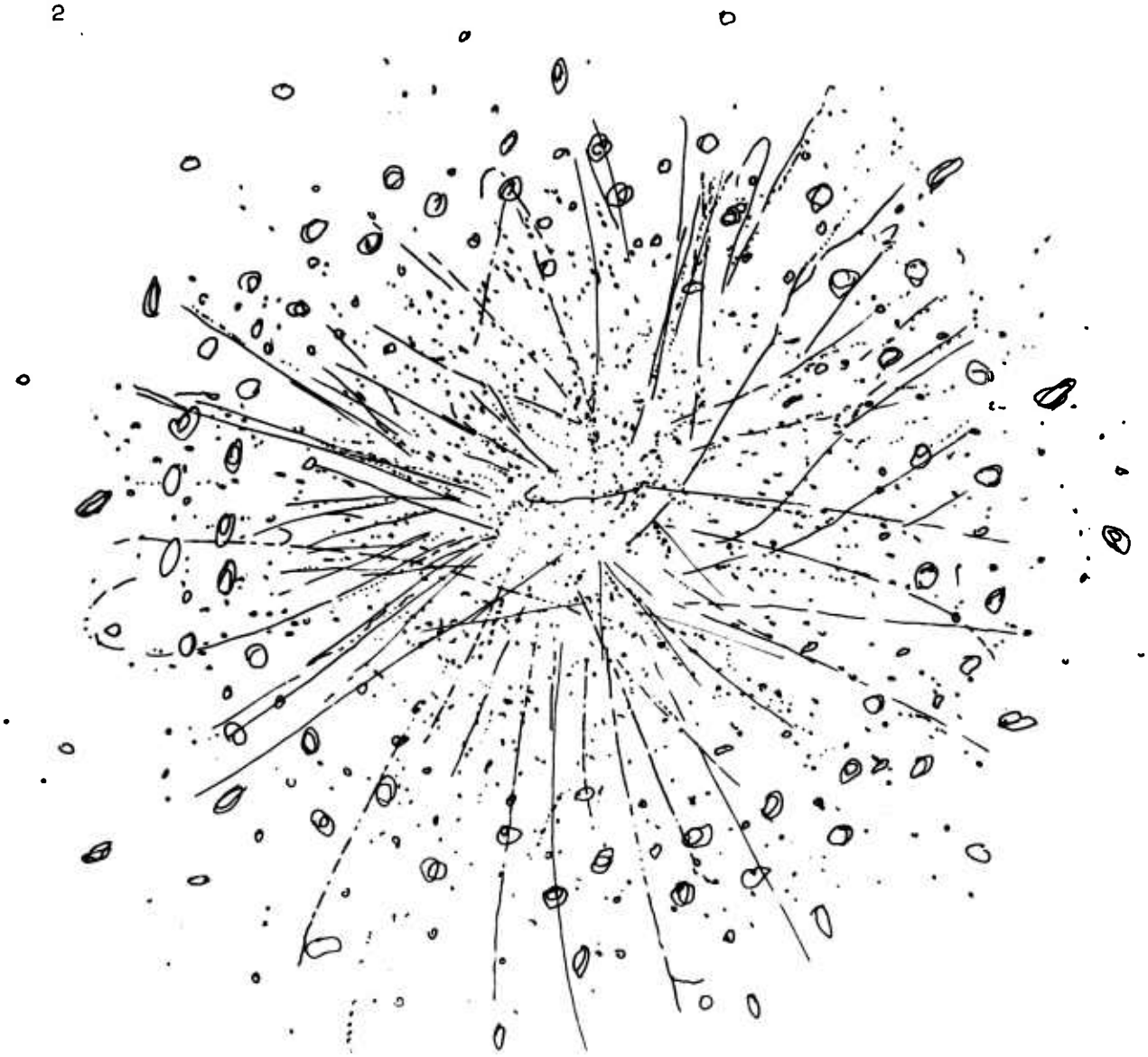

FIGURE 1 Sketch of Spray Pattern from End-on Collision with .020" Al Bumper Plate (12" ahead of witness plate). Zelux Plastic Cylinder .550" Dia., 350" Long, 6 km/sec. Semi Vertex Spray Angle 20°.

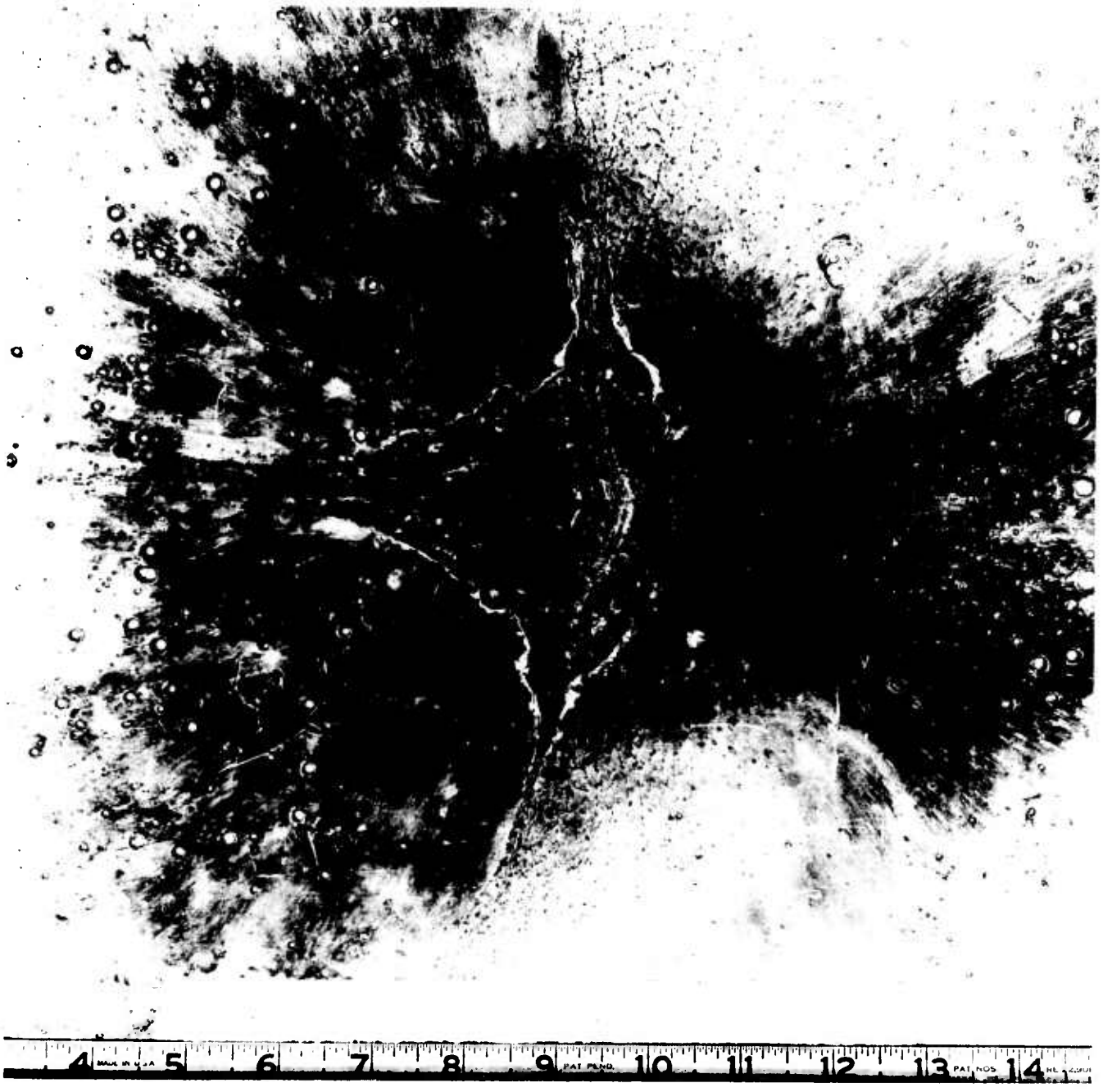

FIGURE 2 Photograph
Spray Pattern from a 0.55" Dia. Plastic Pellet (Cylinder), Striking at Approximately 45°
.020" Al Bumper Plate 12" ahead of Witness Plate, Cylinder Length 0.350"
6 Kilometers/sec.

provide reliable experimental data on shock propagation in solids in circumstances such that vaporization is negligible. The problem of practical interest here concerns the determination of protection effectiveness of thin bumper plates against meteor impact. Pictorially speaking, we may imagine that subsequent to impact, the colliding pellet and entrained bumper material explode, imparting lateral momentum and energy to particles of the pellet at the expense of the original uni-directional pellet momentum. The spreading of the momentum and energy over a relatively large area, combined with the transfer into lateral motion, renders the pellet relatively incapable of further penetration, the exact nature of the damage inflicted on any body behind the bumper being dependent, among other things, on the separation. The central theoretical problem to be considered in this and subsequent reports, is the determination of the translational energy distribution in the spray cross section as a function of the pertinent parameters, viz: distance back of bumper, impact velocity, pellet and bumper material, etc.

The attack on this problem will consist first in determining the initial impact induced states on the basis of one-dimensional theory, (end-on impact of a simple cylinder). Explicit, tractable, analytical expressions will be sought to express the shocked states in terms of the appropriate initial parameters (bumper/pellet density ratio, specific heat ratio, and impact velocity). Radiative loss processes will be delineated to establish the dominant mechanism. Subsequently, the development of a three-dimensional expansion (explosion-like) profile based on the propagation of appropriate rarefaction waves originating at the free-boundaries will be considered on the basis of self-similar motions. Finally, the treatment will be extended to other shapes, and porous materials. This work has been undertaken as part of the Arthur D. Little, Inc., program on space storage of propellants, a program being conducted for NASA. From time to time reports will be issued covering completed phases of the work; this is the first such note and has as its purpose the defining of the problem and method of attack.

II. THE IMPACT MODEL

The impact model may properly be considered in two distinct phases. The first phase establishes the initial shock mechanisms and states along the lines of conventional (References 4,8) one dimensional hydrodynamic shock propagation. To render the problem tractable, the assumption of strong shock wave theory is made in this work, that is, the density ratio is assumed to have reached a limiting value. While this cannot be strictly true, it should provide a reasonable approximation, and enables the derivation of simple expressions for the thermodynamic states generated on impact. The second phase follows the propagation of these initial planar fronts and the explosion-like expansion flow of the vaporized pellet material.

The impact model assumed is illustrated in Figure 3. Conditions just at impact are illustrated in sketch (a); the cylinder of radius r_o strikes the bumper plate at velocity V, the bumper plate thickness δ being much less than r_o. The impact results in the non-stationary wave system illustrated in (b); a transmitted shock $\underset{\rightarrow}{S}_B$ proceeds into the bumper plate at velocity w_B, while a reflected shock $\underset{\leftarrow}{S}_P$ proceeds into the pellet at velocity w_P. The physical functions of these shocks are such as to establish the contact interface in the ideal mechanical model assumed (i.e. that there is no penetration mixing of bumper and pellet material). Thus at the contact plane the bumper shock accelerates the bumper material to a velocity equal to the decreased pellet velocity resulting from $\underset{\leftarrow}{S}_P$. This is defined analytically by the relation:

$$V - u_P = u_B \tag{1}$$

((This simply implies that the pellet and bumper remain in contact.)) Also we have

$$P_B = P_P \tag{2}$$

((I.e. there is no discontinuity of pressure across the contact zone.)) The contact surface $\underset{\rightarrow}{C}$ is then separating bumper and pellet material and traveling to the right at the particle velocity. In many instances (as will emerge from the analysis) all these waves will travel at velocities considerably less than the impact velocity V, in which case all will be swept to the right with respect to an axis system fixed in the bumper. ((In Section VI, Pellet Dynamics, it is pointed out that the rarefaction wave in the bumper will move to the left with respect to an axis system fixed in the bumper, provided γ_B exceeds 2. Note 1 of the foreword indicates the circumstance under which the compression of the pellet may move to the left relative to axes fixed in the bumper.))

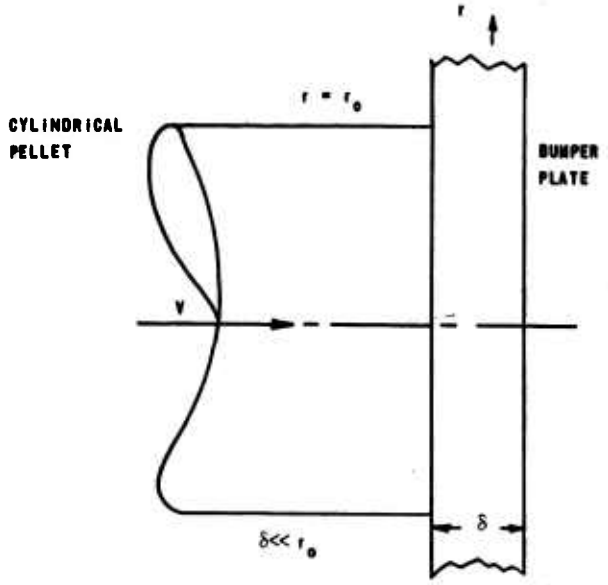

(a)
CONDITIONS AT IMPACT

S_p TRAVELS AT VELOCITY w_p WITH RESPECT TO PELLET, $w_p < V$. ((This implies

$$\left[\left(\frac{\gamma_p + 1}{\gamma_B + 1}\right)\cdot\frac{\rho_{p_o}}{\rho_{B_o}}\right]^{1/2} > 1/2(\gamma_p - 1)$$

See foreword Note 1.))

S_B TRAVELS THROUGH THE BUMPER AT w_B; $w_B < V$.

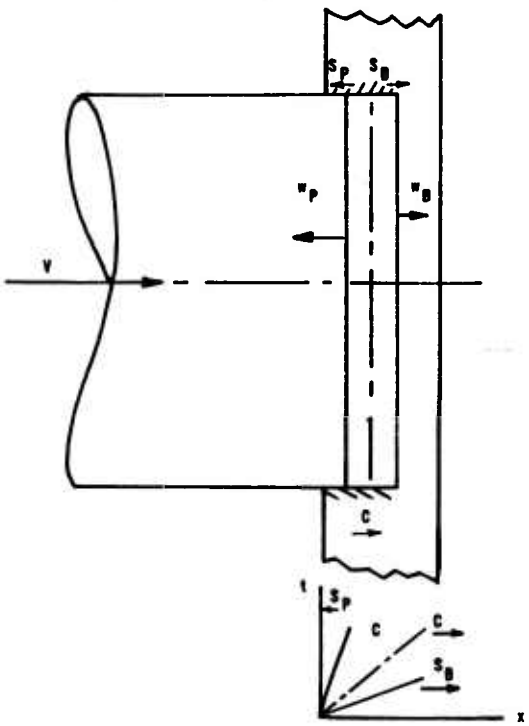

(b)
ASSUMED ONE-DIMENSIONAL CONDITIONS AFTER IMPACT

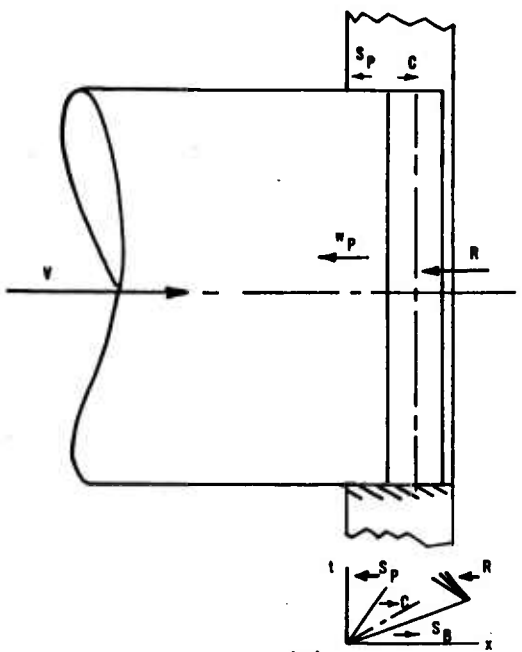

(c)
REFLECTION OF BUMPER SHOCK AS A RAREFACTION, R

FIGURE 3 Assumed Penetrating Geometry

As the impact shocks travel from their origin (i.e. the point of impact), they will in general be diffracted. However, for very thin bumper plates we neglect diffraction effects and assume a one-dimensional wave model as shown in Figure 3, (b) and (c). In this case it is implied that the bumper provides the necessary retaining walls to permit the assumption of one-dimensional flow. Furthermore, shearing stresses are neglected.

When the bumper shock reaches the far surface of the bumper plate, it is reflected as a rarefaction $\underleftarrow{R}$ which proceeds back through the bumper-pellet flow at a velocity $(u - a_P, a_B)$ where u is the particle velocity to the right, again in space-fixed coordinates. ((This rarefaction $\underleftarrow{R}$ will move to the left or to the right in space-fixed coordinates according as γ_B is greater than or less than 2--See Section VI.)) $\underleftarrow{R}$ will eventually overtake and cancel $\underrightarrow{S_P}$, thus if the pellet is long enough relative to the bumper thickness, a portion of the pellet would remain intact after penetrating the bumper. If $\underleftarrow{R}$ actually moves to the right in space-fixed coordinates (requiring that $\gamma_B < 2$) then the compressed regions of the pellet and bumper can protrude through the bumper; in this case the restraint afforded by the bumper will cease to exist at the rear face of the bumper and a cylindrical rarefaction $\downarrow R$ will be formed as this restraint is relaxed. The resulting model is shown in Figure 9(b); both the rarefaction $\underleftarrow{R}$ and $\downarrow R$ accelerate the material to escape speed. In this case the inward facing rarefaction waves $\downarrow R_c$ are accelerating particle flow radially and attenuating the pellet shock $\underrightarrow{S_P}$; these cylindrical wave fronts proceed radially inward at the local velocity of sound, a_P, a_B, and are assumed to cancel in all regions where they intersect $\underleftarrow{R}$. Thus $\underleftarrow{R}$ accelerates the flow axially, while $\downarrow R_c$ produces radial acceleration; the amount and nature of material accelerated in both directions depends on the relative velocities and geometrics of these two fronts.

Thus it is seen in this assumed model that on impact the kinetic energy of the pellet is transferred partially into kinetic energy of the affected regions of the bumper plate and partially into thermodynamic energy of both pellet and bumper material. The energy transfer is effected through the transmitted and reflected shock waves. A large portion of the thermodynamic energy imparted to the pellet and displaced bumper material is ultimately transferred to kinetic energy through a series of expansion waves originating at the boundaries. The remainder of the thermodynamic energy is involved with the vaporization energies of the materials.

((The case of $\gamma_B > 2$ in which the rarefaction wave accelerates the material to less than escape velocity and subsequent expansion occurs at the rear surface of the bumper where the cylindrical constraint is released requires a somewhat more complicated model. This case is shown in Figure 8.))

III. THE CONSERVATION RELATIONS

The analysis is based on negligible shear forces, i.e. a compressible fluid is assumed. The mass and momentum conservation relations may be written in the usual form; where it is assumed that the fluid remains ideal:

$$\left.\begin{aligned} \rho_{B_o} w_B &= \rho_B (w_B - u_B) \\ P_{B_o} + \rho_{B_o} w_B^2 &= P_B + \rho_B (w_B - u_B)^2 \end{aligned}\right\} \quad \text{across the bumper shock} \qquad (3)$$

and

$$\left.\begin{aligned} \rho_{P_o} w_P &= \rho_P (w_P - u_P) \\ P_{P_o} + \rho_{P_o} w_P^2 &= P_P + \rho_P (w_P - u_P)^2 \end{aligned}\right\} \quad \text{across the pellet shock} \qquad (4)$$

The symbols are self-evident from Figure 4.

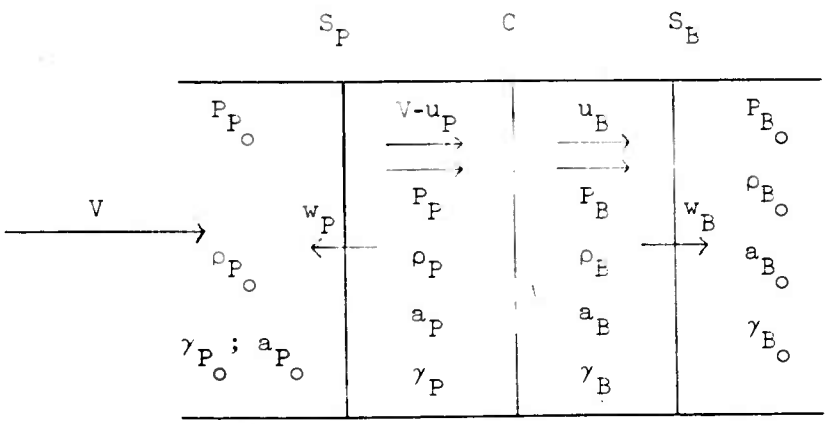

Figure 4

Equations 3 and 4 can be combined and algebraically arranged to yield the normal expressions for shock wave and particle velocity:

$$w_B = \sqrt{\frac{\rho_B (P_B - P_{B_o})}{\rho_{B_o}(\rho_B - \rho_{B_o})}}, \qquad w_P = \sqrt{\frac{\rho_P}{\rho_{P_o}} \frac{P_P - P_{P_o}}{\rho_P - \rho_{P_o}}} \tag{5}$$

$$u_B = \sqrt{\frac{(P_B - P_{B_o})(\rho_B - \rho_{B_o})}{\rho_B \rho_{B_o}}}, \qquad u_P = \sqrt{\frac{(P_P - P_{P_o})(\rho_P - \rho_{P_o})}{\rho_P \rho_{P_o}}} \tag{6}$$

The pressure relations may be derived directly also:

$$P_B - P_{B_o} = \rho_{B_o} w_B^2 - \rho_B (w_B - u_B)^2$$

$$= \rho_B u_B (w_B - u_B) = \rho_{B_o} w_B u_B$$

and since the undisturbed pressures may in all cases be regarded as negligible in comparison with the shocked pressures, using (2) we may write simply:

$$P_P = P_B = \rho_{B_o} w_B u_B = \rho_{B_o} w_P u_P \tag{7}$$

By using (3) and (4) we may write the appropriate conservation of energy relations as:

$$e_B - e_{B_o} = 1/2 \left\{ P_B + P_{B_o} \right\} \left\{ \frac{1}{\rho_{B_o}} - \frac{1}{\rho_B} \right\} \tag{8}$$

$$e_P - e_{P_o} = 1/2 \left\{ P_P + P_{P_o} \right\} \left\{ \frac{1}{\rho_{P_o}} - \frac{1}{\rho_P} \right\} \tag{9}$$

where the latent heat of vaporization has been neglected. ((This neglect of the heat of vaporization implies that we are considering very high

energy processes such as are experienced in meteoric impact; the experimental data obtained in hypervelocity firings pertain to lower velocity impacts in which this simplification is inappropriate.)) To sufficient accuracy these may be written as:

$$e_B - e_{B_o} = 1/2\ P_B\left\{\frac{1}{\rho_{B_o}} - \frac{1}{\rho_B}\right\} \tag{10}$$

$$e_P - e_{P_o} = 1/2\ P_P\left\{\frac{1}{\rho_{P_o}} - \frac{1}{\rho_P}\right\} \tag{11}$$

For polytropic gases, the enthalpy may be written as $(\gamma/\gamma\text{-}1)\cdot(P/\rho)$ and the standard Rankine-Hugoniot pressure-density relations derived:

$$\frac{P_P}{P_{P_o}} = \frac{\dfrac{\gamma_{P_o}+1}{\gamma_{P_o}-1} - \dfrac{\rho_{P_o}}{\rho_P}}{\dfrac{\gamma_P+1}{\gamma_P-1}\dfrac{\rho_{P_o}}{\rho_P} - 1}, \qquad \frac{P_B}{P_{B_o}} = \frac{\dfrac{\gamma_{B_o}+1}{\gamma_{B_o}-1} - \dfrac{\rho_{B_o}}{\rho_B}}{\dfrac{\gamma_B+1}{\gamma_B-1}\dfrac{\rho_{B_o}}{\rho_B} - 1} \tag{12}$$

which defines the limiting density ratio for very strong shock waves as:

$$\lim_{\frac{P_P}{P_{P_o}} \longrightarrow \infty}\left(\frac{\rho_P}{\rho_{P_o}}\right) = \frac{\gamma_P+1}{\gamma_P-1}, \qquad \lim_{\frac{P_B}{P_{B_o}} \longrightarrow \infty}\left(\frac{\rho_B}{\rho_{B_o}}\right) = \frac{\gamma_B+1}{\gamma_B-1} \tag{13}$$

Based on the assumption that the impact shocks are very strong, (13) may be applied to yield the following relations:

a. Particle velocity ratio:

$$\frac{u_B}{u_P} = \sqrt{\frac{\gamma_P+1}{\gamma_B+1}\frac{\rho_{P_o}}{\rho_{B_o}}} \tag{14}$$

b. Particle velocity behind the shock: (combine Equations 1 and 14.)

$$u_B = \frac{V}{1 + \sqrt{\frac{\gamma_B + 1}{\gamma_P + 1} \frac{\rho_{B_o}}{\rho_{P_o}}}} \tag{15}$$

c. Shock wave velocities (combine Equations 5 and 13).

$$w_B = \frac{\gamma_B + 1}{2} u_B, \quad w_P = \frac{\gamma_P + 1}{2} u_P \tag{16}$$

d. Pressure in shocked states:

$$P_P = P_B = \frac{\gamma_B + 1}{2} \rho_{B_o} \frac{V^2}{\left[1 + \sqrt{\frac{\gamma_B + 1}{\gamma_P + 1} \frac{\rho_{B_o}}{\rho_{P_o}}}\right]^2} \tag{17}$$

e. Temperature in shocked states:

This may be obtained by combining the strong shock relations with (10) and (11), using (17), and assuming the ideal gas relation $e = c_v T$:

$$T_B - T_{B_o} = \frac{\gamma_B - 1}{2R_B} \frac{V^2}{\left[1 + \sqrt{\frac{\gamma_B + 1}{\gamma_P + 1} \frac{\rho_{B_o}}{\rho_{P_o}}}\right]^2}$$

or to sufficient approximation:

$$T_B = \frac{\gamma_B - 1}{2R_B} \frac{V^2}{\left[1 + \sqrt{\frac{\gamma_B + 1}{\gamma_P + 1} \frac{\rho_{B_o}}{\rho_{P_o}}}\right]^2} \tag{18}$$

and similarly:

$$T_P = 1/2 \frac{\gamma_P - 1}{R_P} \frac{\rho_{B_o}}{\rho_{P_o}} \frac{\gamma_B + 1}{\gamma_P + 1} \frac{V^2}{\left[1 + \sqrt{\frac{\gamma_B + 1}{\gamma_P + 1} \frac{\rho_{B_o}}{\rho_{P_o}}}\right]^2} \tag{19}$$

f. The velocity of sound in the shocked states may be derived from the polytropic relation $a^2 = \gamma_P/P$, yielding:

$$a_B = \sqrt{\frac{\gamma_B(\gamma_B - 1)}{2}} \frac{V}{1 + \sqrt{\frac{\gamma_B + 1}{\gamma_P + 1} \frac{\rho_{B_o}}{\rho_{P_o}}}} \tag{20}$$

$$a_P = \sqrt{\frac{\gamma_P(\gamma_P - 1)(\gamma_B - 1)}{2(\gamma_P + 1)} \frac{\rho_{B_o}}{\rho_{P_o}}} \frac{V}{1 + \sqrt{\frac{\gamma_B + 1}{\gamma_P + 1} \frac{\rho_{B_o}}{\rho_{P_o}}}} \tag{21}$$

g. The shock Mach number may be written simply as:

$$\frac{w_B}{a_B} = \sqrt{\frac{(\gamma_B + 1)^2}{2\gamma_B(\gamma_B - 1)}}, \text{ and } \frac{w_P}{a_P} = \sqrt{\frac{(\gamma_P + 1)^2}{2\gamma_P(\gamma_P - 1)}} \tag{22}$$

Equations 14 to 22, inclusive, completely define the impact induced thermodynamic states.

IV. SOME NUMERICAL EXAMPLES

In the subsequent analysis of three-dimensional motion, it is of prime importance to know the practical range of conditions to be encountered behind the impact shocks. In the condensed states, such as are encountered behind the impact shocks, considerable uncertainty arises as to the value of γ to be chosen. In the subsequent calculations, quantities will be expressed in terms of γ under the assumption that $\gamma_P \approx \gamma_B$, so that

$$\frac{\gamma_B + 1}{\gamma_P + 1} \approx 1,$$

but since γ_P, γ_B may approach unity, the inequality

$$\frac{\gamma_B - 1}{\gamma_P - 1} \neq 1,$$

will be observed.

Various quantities estimated in Equations 14 to 22 have been evaluated; these are plotted in Figures 5, 6, and 7.

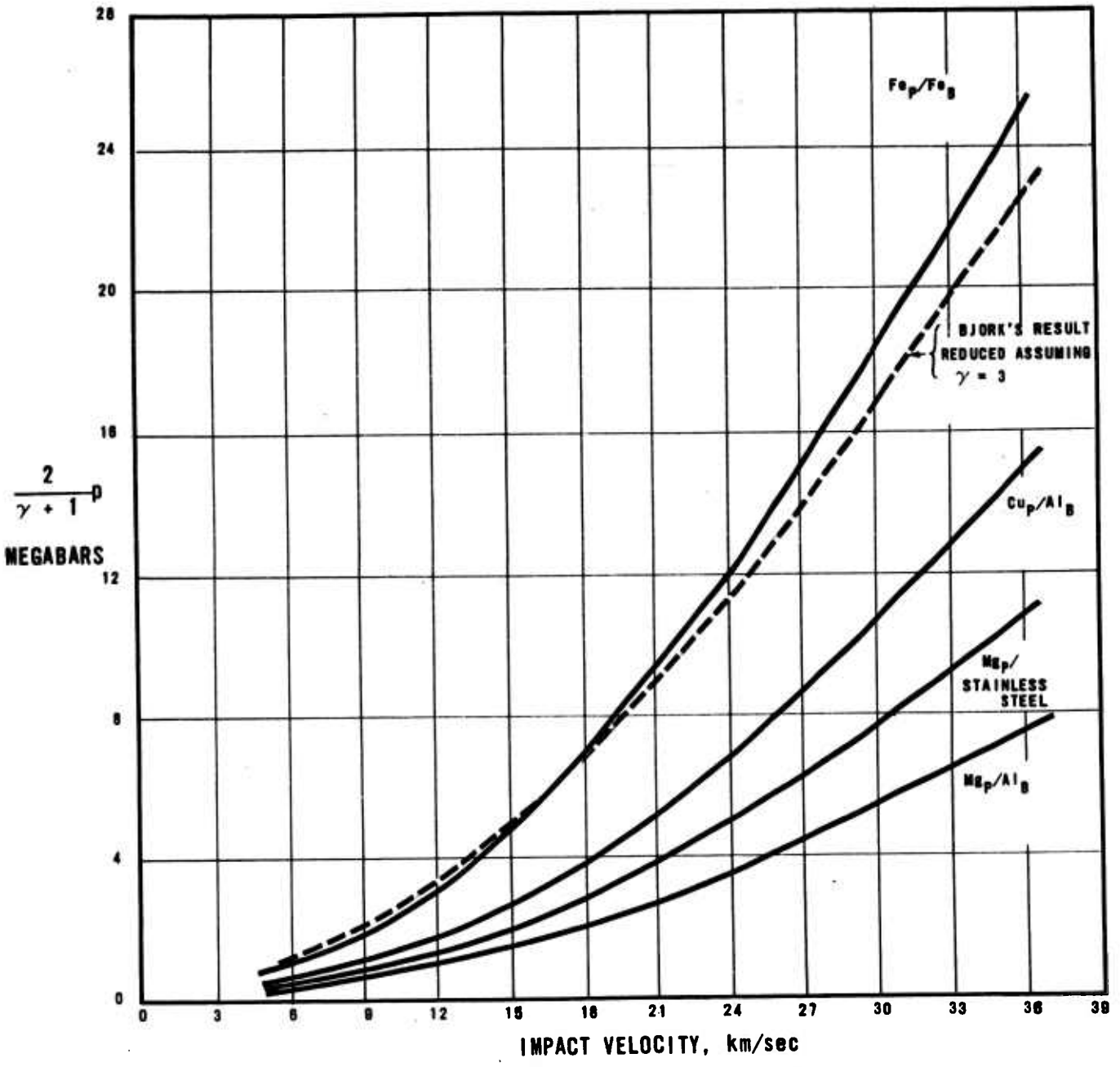

FIGURE 5 Impact Pressures from Equation $\gamma_P \simeq \gamma_B$

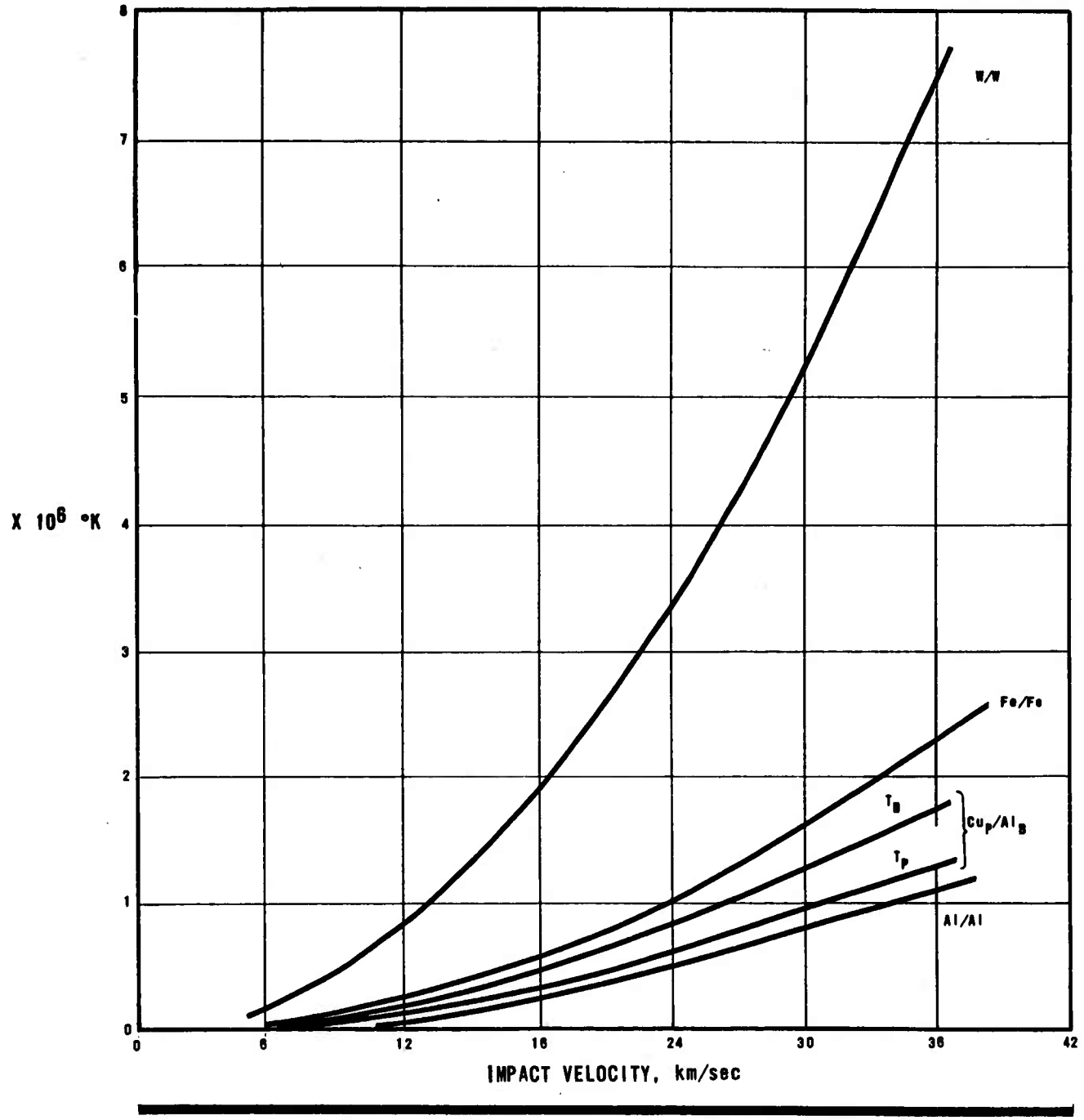

FIGURE 6 Impact Temperatures

$\gamma = 3$

$\gamma_B = \gamma_P$

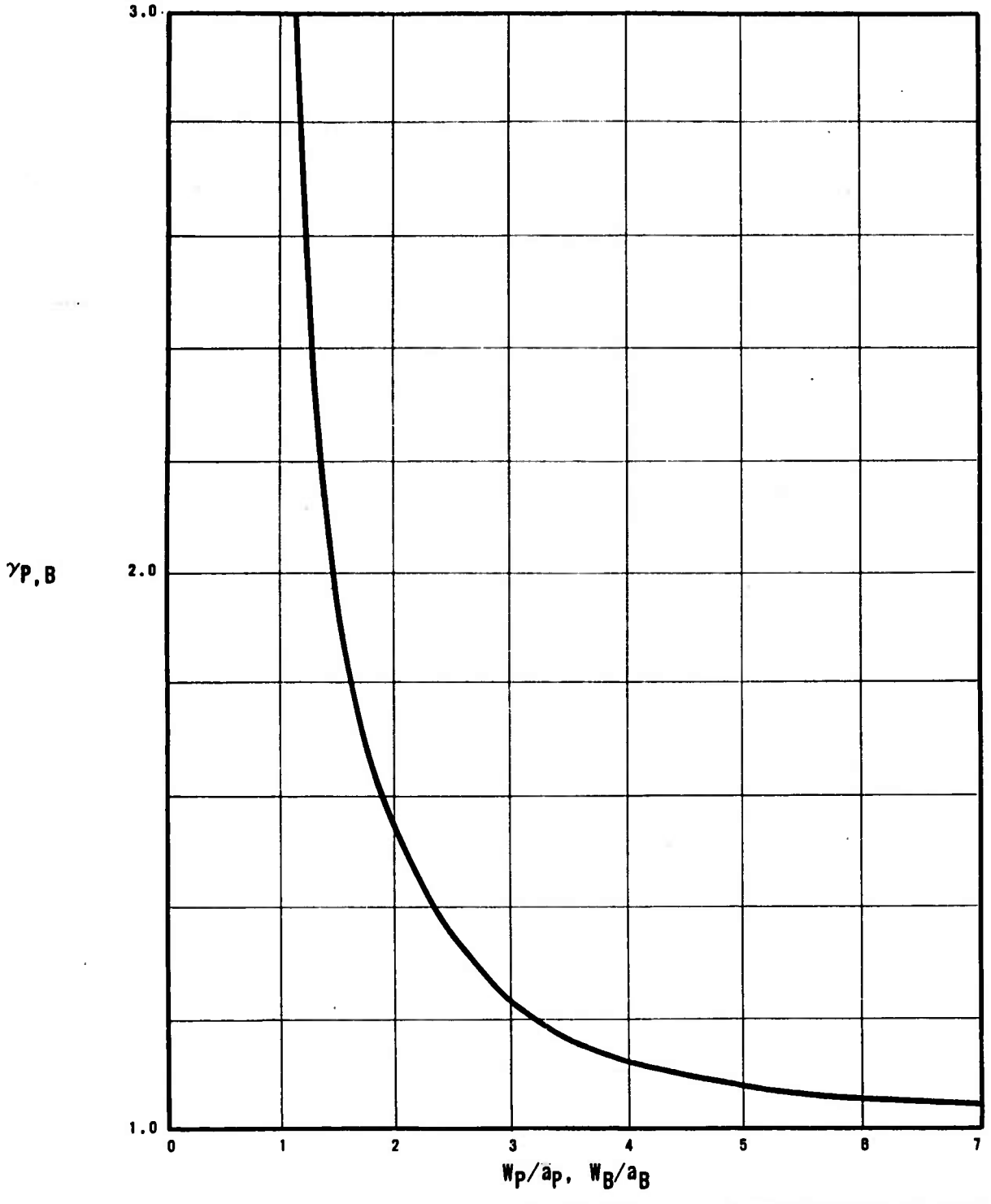

FIGURE 7 Shock Mach Number

V. DISCUSSION OF RESULTS

One of the most important assumptions (aside from that of ideal fluid behavior) is the use of the strong shock approximation, i.e. the use of the limiting density ratio. The rigorous justification of such an approximation is obviously not possible. Its effect must be estimated in relation to each parameter.

A. PRESSURE RESULTS

The pressure is plotted in Figure 5 for a range of cases; the effect of initial density ratio may be seen by comparison of the magnesium into aluminum case (Mg_P/Al_B) with the copper into aluminum case (Cu_P/Al_B); one finds a doubling of pressure ratio in the case of the heavier metal impacting pellet.

In these plots γ has been used as a parameter multiplying pressure. It may be observed that for condensed media, the appropriate value of γ is generally accepted as 3 (see references 4 and 8). An interesting comment may be made on this value by examining Equation 17 for the impact of similar materials, in which case

$$p = \frac{\gamma + 1}{2} \rho_o \left(\frac{V}{2}\right)^2$$

which with $\gamma = 3$ reduces to the well-known expression used by many authors for impact pressure:

$$p = \frac{1}{2}\rho_o V^2.$$

It may be seen by consideration of the exact Rankine-Hugoniot equations relating pressure ratio to density ratio across a shock, that for large values of γ the limiting density ratio is rapidly attained. Thus for $\gamma = 3$ one would expect reasonable pressure predictions using the strong shock assumption. Bjork (Reference 3, Figure 4) quotes a computed pressure variation for iron impacting onto iron as $p = 0.120\ V^{1.64}$ where p is in megabars and V in km/sec. This value has been included in Figure 5 for comparison with the Fe_P/Fe_B pressures predicted by Equation 17. In plotting Bjork's formula, the pressures have been reduced to correspond to the case $\gamma = 3$. The agreement with the predictions of Equation 17 may be observed to be good.

Experimental measurements of shocked pressures in metals are few. Among the most extensive studies were those of the Los Alamos Laboratory

(References 5,6,7). Unfortunately, driver free-surface velocity is not given in their reports, so that only qualitative comparison can be made. In this case it can be seen that based on a $\gamma = 3$, and assuming $\gamma_P = \gamma_B$, an impacting steel plate will generate 1 megabar shocks in a brass specimen at an impact velocity of approximately 14,000 fps and 1.5 megabar shocks at an impact velocity of approximately 17,000 fps.

B. TEMPERATURE IN SHOCKED STATES

Temperatures in the shocked state as given by Equations 18 and 19 have been plotted in Figure 6. It is interesting to note the simple form of the temperature relation when similar materials collide:

$$T_B = T_P = \frac{\gamma - 1}{8R} V^2.$$

The temperatures calculated directly from the analytical relations do not take into account the energy absorbed in breaking the crystal lattice and vaporization. Using the values quoted by the Russian workers (Reference 9, page 307):

Medium	Energy Density of Crystal Lattice Including Latent Heat of Fusion ergs/gm	Vaporization Energy ergs/gm
Sand	5×10^9	
Granite	7×10^9	2×10^{10}
Aluminum	4×10^9	10^{11}
Iron	3×10^9	7×10^{10}

The predicted temperatures may be reduced to allow for the vaporization energy, where the decrease in the latent energies with temperature must be properly taken into account. When these calculations are performed, it is found that negligible decreases in temperature occur at the higher temperatures where this theory is essentially applicable; the main modifications occur at the lower end of the velocity range, and here the Deybe model along with the Mie-Grunïesen equation of state as applied in References 5,6,7, yields temperatures approximately one order of magnitude lower than predicted by the theory presented here. Generally speaking, it would be expected that above 10 km/sec the vaporization energy may be neglected and the predictions of the simple theory considered valid other than as limited by the ideal type behavior assumed.

The simple expression quoted above for impact temperatures when similar materials collide, shows that the temperature rise (γ assumed the

same in all cases) varies between materials directly as the molecular weight. Thus the three curves Al/Al, Fe/Fe, and W/W of Figure 6 reflect simply the molecular weight changes. The more complex expressions involved when different metals collide yields the simple relation between pellet and bumper temperatures:

$$\frac{T_P}{T_B} = \frac{R_B}{R_P}\frac{\rho_{B_o}}{\rho_{P_o}} = \frac{(\text{Mol.Wt.})_P}{(\text{Mol.Wt.})_B}\frac{\rho_{B_o}}{\rho_{P_o}}$$

The extremely high temperatures predicted naturally indicate the break-down of the simple ideal theory used here. First as the high temperatures are approached, electrons will be stripped off the atoms, yielding, of course, a lower gas-kinetic temperature, and requiring the application of a Thomas-Fermi equation for the condensed state. In the second instant, with the high temperatures achieved, it is apparent that radiative processes will tend to dominate the early phases. ((Bremsstrahlung and absorption-re-emission may well prove to be important mechanisms for transporting energy from the shocked interior to the radiating surface.)) The gas flow processes will occur relatively at a much slower rate until the extreme temperatures have been dissipated. Both the above comments lead to the added complexity of non-negligible departures from local thermodynamic equilibrium, while inherent in the simple model here is the assumption of a Maxwellian distribution.

Experimental evidence to date on impact flash temperature is practically non-existant; a few spectra have been taken, as well as some long wave length radiometric observations, but only general qualitative remarks can be made on these observations. The intensity of the radiation throughout the visible and near visible regions, even at low impact velocities (6-7 km/sec), is attested to by the clarity of the image left on an exposed photographic plate (shutter left open), the motion of the pellet being frozen at the impact condition by its own impact flash. Rather intense X-band pulses have been recorded on impact in this velocity range; a black-body calculation would indicate a radiant intensity (based on a pellet length of shocked gas $\div \delta$) of the order of a few microwatts in this frequency range for temperatures of the order of 10^6°K. Observations have shown considerably larger emissions at these long wave lengths (3 cm), and these have been attributed tentatively to Bremsstrahlung. Total thermal intensities may be shown to be quite large based on the ideal model (of the order of 10^8 to 10^{12} watts). Thus the tentative interesting observation may be made that as real gas effects are introduced and the gas-kinetic temperature drops, the power emitted tends to increase in the long wave length regions. At the same time, of course, departures from local thermodynamic equilibrium become important.

VI. PELLET DYNAMICS AND WAVE GEOMETRY

The one-dimensional status may be assumed to exist until the bumper shock has reached the far side of the bumper plate, at which time it will be reflected as a rarefaction centered about this rear face. Under the assumptions of the theory, the rear face would then be accelerated instantaneously to escape velocity, and the rarefaction spreading out as it progresses would travel back through the bumper-pellet at a velocity $u_{B,P} - a$. Two conditions are of interest here. First, if the front of the rarefaction travels upstream through the condensed media at a velocity greater than the local particle velocity, then the rarefaction will never pass downstream of the rear bumper surface, and in effect we would have the media issuing from a cylindrical orifice with the initial front velocity approaching escape speed and gradients appropriate to the centered rarefaction, with the gas column expanding laterally to adjust to the boundary conditions of free space. This condition is illustrated crudely in Figure 8.

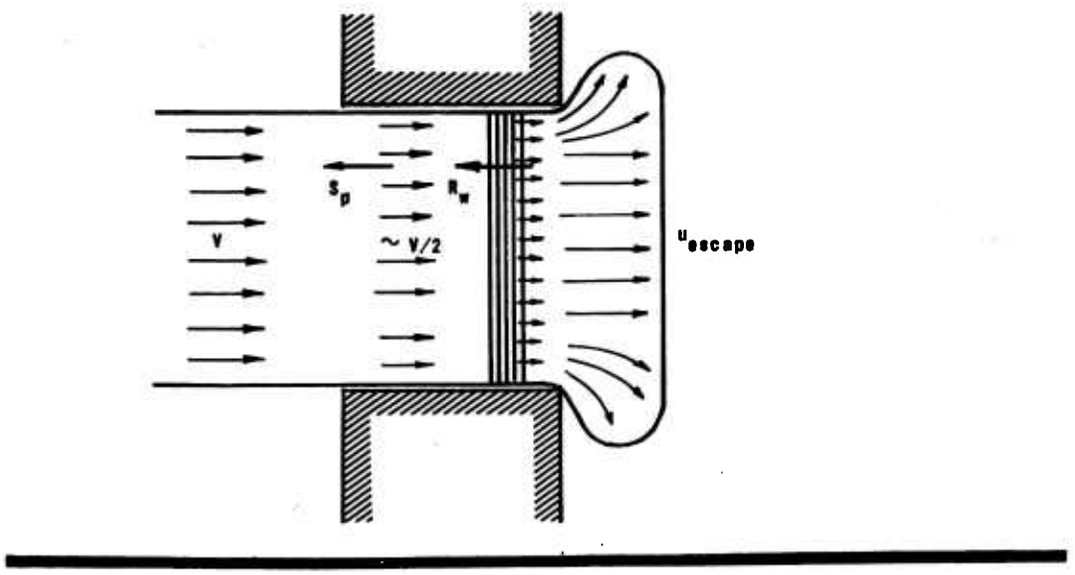

FIGURE 8

The analytical condition for which this state of affairs may be expected can be expressed by comparing Equations 15 and 20, and it may be seen that the requirement is:

$$\frac{\gamma_B(\gamma_B - 1)}{2} > 1$$

or:

$$\gamma_B > 2$$

If $\gamma_B > 2$, then it is apparent that the front of the rarefaction wave will be swept past the rear face of the bumper and the restraint on the boundary of the shocked volume contained between $\overleftarrow{S}_B$ and $\overleftarrow{R}_w$ suddenly released. Under these conditions, it would appear a reasonable first-try approximation to assume that the bumper plate is removed instantaneously from the picture, having established in the pellet a pulse of one-dimensional, shocked, condensed media, of width somewhat less than twice the bumper plate thickness. Thus we imagine that at the instant the bumper impact shock reaches the far surface of the bumper plate, all restraint is removed on the pellet boundaries, and the wave geometry appropriate to this assumption is illustrated in Figure 9(a). At this instant a plane centered rarefaction wave $\overleftarrow{R}_w$ starts upstream through the pellet and must overtake the pellet shock $\overleftarrow{S}_B$ eventually (if the pellet is sufficiently long).

In addition, a centered cylindrical rarefaction $\downarrow R_c$ must start at the free boundary and progress inwards towards the center of the pellet, imparting radial acceleration to the condensed media. After some time, the wave system in the pellet will have assumed the form shown in Figure 9(b).

Radial outflow will be initiated by the passage of the impact shock and stopped by the arrival of the end rarefaction wave. Expansion waves from the cylindrical boundaries will be propagated throughout the field, overtaking and decaying at least part and possibly all of the impact shock before the arrival of the end rarefaction. This diffraction at the edge of the impact shock is illustrated in Figure 9(b). The pellet flow regions may be divided then as follows:

a. A one-dimensional field of axial high velocity gas flow behind the plane portion of the end rarefaction (Region 1 in Figure 9(b)).

b. A one-dimensional field of axial lower velocity flow behind the planar portion of the impact shock and the boundaries of $\downarrow R_c$, (Region 2 of Figure 9(b)).

c. A more or less radial outflow field ahead of the front $\overleftarrow{R}_w$, established by $\downarrow R_c$ (Region 3 of Figure 9(b)).

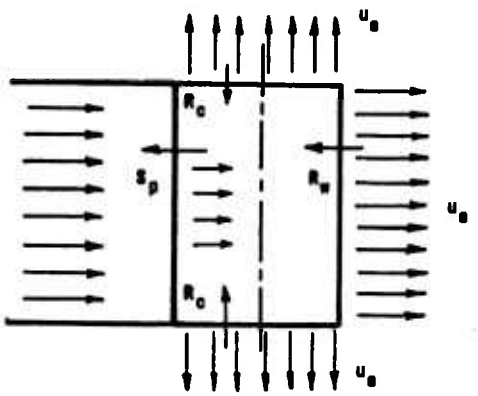
u_s
R_c
S_p
R_w
u_s
R_c
u_s

a

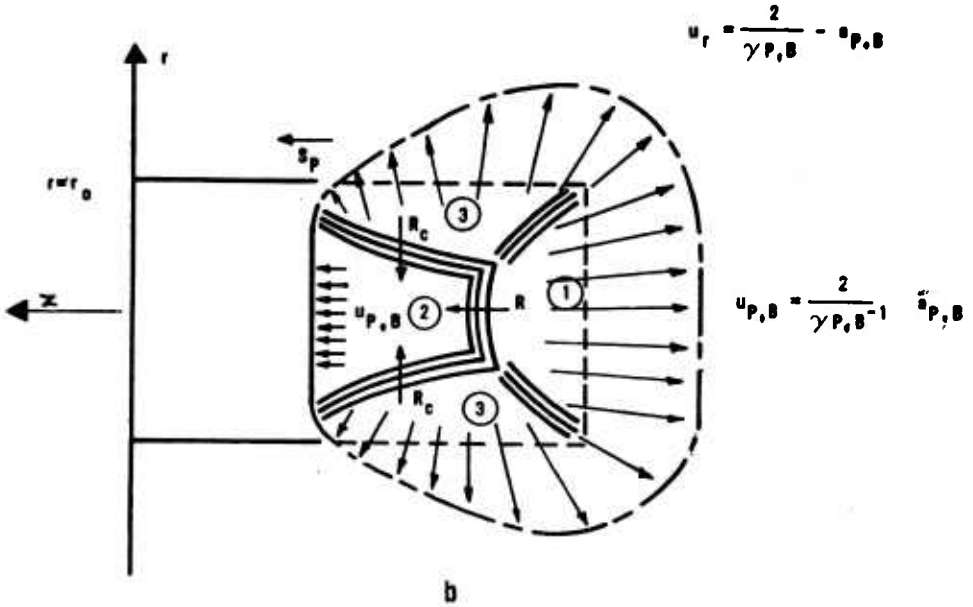
$u_r = \frac{2}{\gamma P,B} - a_{P,B}$
r
$r=r_o$
S_p
R_c
3
z
$u_{P,B}$
2
R
1
$u_{P,B} = \frac{2}{\gamma P,B - 1}\ a_{P,B}$
R_c
3

b

FIGURE 9

d. An interaction field joining the axial flow region (1) to the radial flow region (3), established by the interaction between $\downarrow R_c$ and $\overleftarrow{R_w}$.

e. An interaction field joining the radial field (3) with the axial field (2) and established by the interaction of edge-rarefactions with the impact shock.

The detailed solution of each of these fields is beyond the scope of this present note and will be treated in subsequent reports. There are, however, some interesting simple points that might be made without too much complexity of analysis. In the first instance, one is led to wonder how soon the impact shock will be decayed, either by cylindrical edge disturbances or by the overtaking of $\overleftarrow{R_w}$.

The edge disturbance may be considered in a simple geometrical manner with reference to Figure 10, where the conditions are shown an infinitesimal time after the release of side-wall restraint. An axis system is shown fixed in the pellet at the time of release.

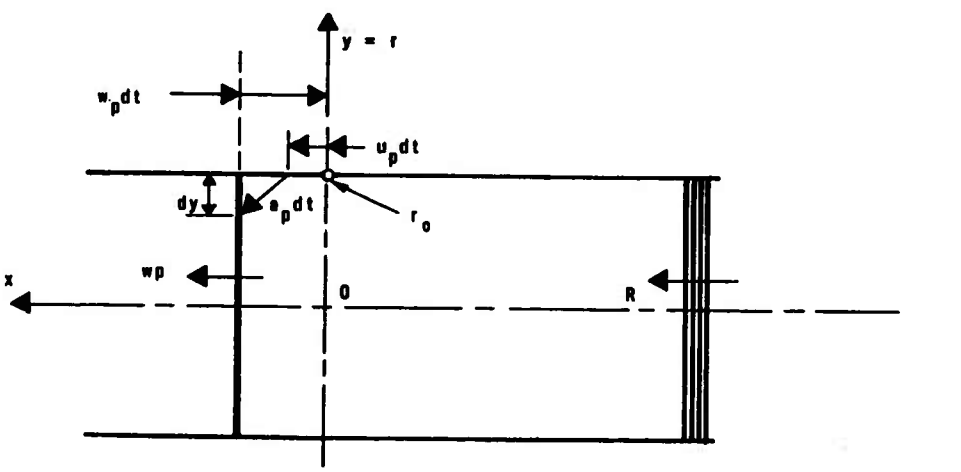

FIGURE 10

The expansion disturbance originating at (0, r_o) will be translated behind the shock at velocity u_P, and will penetrate in and interact with the shock to a depth dy. The differential equation defining this inner point of interaction is:

$$\frac{dy}{dx} = \frac{\sqrt{a_P^2 - (w_P - u_P)^2}}{w_P}$$

which can be integrated (assuming a_P, w_P, u_P constant) to yield:

$$y = \frac{x\sqrt{a_P^2 - (w_P - u_P)^2}}{w_P}$$

which on substitution of Equations 14, 15, 16, and 21 yields:

$$\frac{y}{x} = \sqrt{\frac{\gamma_P - 1}{\gamma_P + 1}}$$

These sidewaves will have penetrated to the pellet axis (and hence attenuated the whole wave $\overleftarrow{S}_P$) at:

$$x = \frac{r_o}{\sqrt{\frac{\gamma_P - 1}{\gamma_P + 1}}}$$

which for $\gamma_P = 3$, is approximately 1.5 radii. Thus we are in effect saying that the shock diffraction effects are confined to a small portion of the planar front for bodies whose lengths are less than their diameters.

The end originating rarefaction $\overleftarrow{R}$ will overtake and interact (tending to cancel) the pellet impact shock wave. This may be expected to be the most important cancellation process, where lateral dimensions are of at least the same order of magnitude as longitudinal pellet dimensions. The position in the pellet for which overtaking will occur may be computed from the simple geometry of Figure 11.

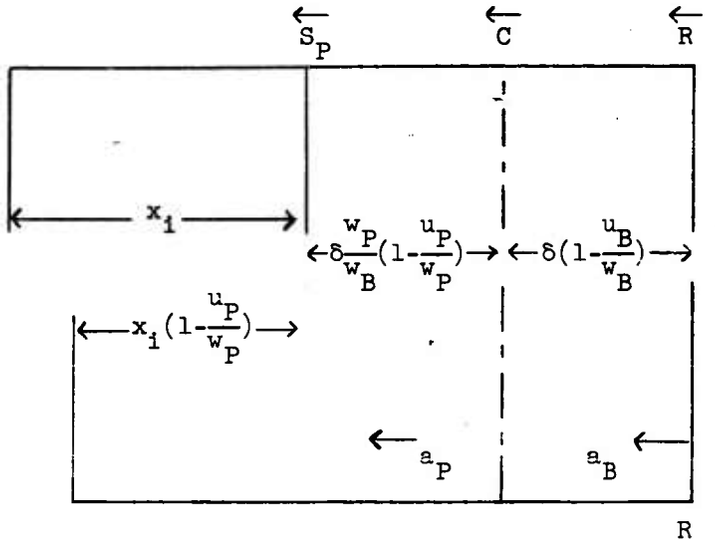

Figure 11

In Figure 11, x_i denotes the length of pellet which must enter the shock wave S_P from the time the rarefaction wave is first formed until it overtakes the shock. The pellet of length x_i will be compressed to $x_i(1 - u_P/w_P)$ on passing through the shock wave. Equating the times for the shock and the rarefaction to merge, one has

$$\frac{x_i}{w_P} = \frac{\delta}{a_B}\left(1 - \frac{u_B}{w_B}\right) + \frac{\delta}{a_P}\cdot\frac{w_P}{w_B}\left(1 - \frac{u_P}{w_P}\right) + \frac{x_i}{a_P}\cdot\left(1 - \frac{u_P}{w_P}\right)$$

Upon substitution of the appropriate relations from Equations 14 to 22, one obtains

$$\frac{x_i}{\delta} = \frac{\sqrt{\frac{\rho_{B_o}(\gamma_P + 1)}{\rho_{P_o}(\gamma_B + 1)}}\left[\sqrt{\frac{\gamma_P(\gamma_B - 1)}{\gamma_B(\gamma_P - 1)}} + 1\right]}{\sqrt{\frac{2\gamma_P}{\gamma_P - 1}} - 1} \tag{23}$$

wherein substitution of $\gamma_P = \gamma_B = \gamma$ yields

$$\frac{x_i}{\delta} = \frac{2\sqrt{\frac{\rho_{B_o}}{\rho_{P_o}}}}{\sqrt{\frac{2\gamma}{(\gamma - 1)}} - 1}$$

This function has been plotted in Figure 12 as a function of γ and initial density ratio, and it may be observed that overtaking occurs in quite a short distance, probably within ten times the bumper plate thickness, in the most probable region of interest. The interaction of an overtaking rarefaction with a shock wave has been discussed by several authors (Reference 11), but is complicated in this case by degeneracy into elastic shocks.

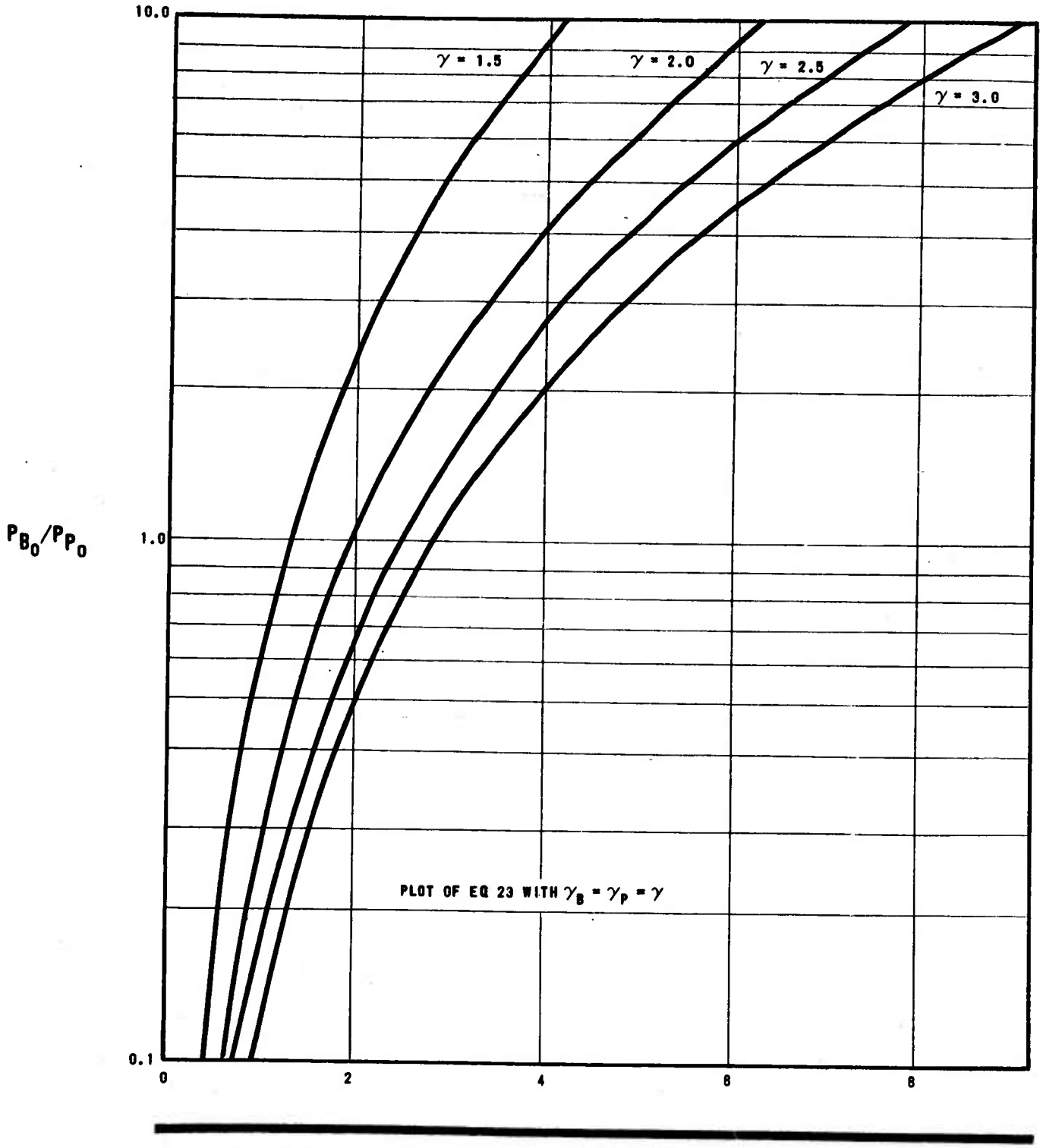

FIGURE 12 Overtaking Point Measured from Initial Position of S_P at Time S_B Reaches far Side of Bumper

VII. RADIAL FLOW

As previously stated, the band of highly shocked gas between the wave fronts $\underleftarrow{S}_P$ and $\underleftarrow{R}$ will start to expand radially as soon as the sidewall pressure is released, i.e. at the rate the boundary is swept by the rear bumper surface. For the first approximation we have assumed instantaneous release of the restraint on the sidewall so that radial outflow starts at the shock wave $\underleftarrow{S}_P$. The detailed geometry was shown in Figure 9(b). The reference axis chosen is fixed in the pellet at the undisturbed end. With respect to this axis system, $\underleftarrow{S}_P$ induces a particle velocity u_P in the negative direction. The inward traveling rarefaction $\downarrow R_c$ accelerates the flow approximately radially, and since it is centered with its origin at $r = r_o$, then:

$$u_{r_o} = \frac{2}{\gamma_{P,B} - 1} \, a_{P,B}$$

where it is assumed that the polytropic exponent γ may be approximated by a constant average value. In practice it is known that condensed media on expansion must follow a more complicated form where $\gamma = \gamma(p,T)$, γ assuming its isentropic value only after considerable expansion (Stanyukovich suggests for $p < 10^4$ atmospheres). This problem will be considered in detail in a subsequent paper.

Since the flow in this region is translating with a velocity u_B, the envelope of the expansion products will be a cone with semi-vertex angle:

$$\phi = \tan^{-1} \frac{u_{r_o}}{u_B} = \tan^{-1} \frac{2}{\gamma_{P,B} - 1} \frac{a_{P,B}}{u_B}$$

(the subscripts defining the envelopes for the two different materials). See Note 2 of foreword.

Using the previously derived relations, this may be written as:

$$\phi_B = \tan^{-1} \sqrt{\frac{2\gamma_B}{\gamma_B - 1}} \qquad (24)$$

for the bumper material, and:

$$\phi_P = \tan^{-1}\sqrt{\frac{2\gamma_P}{\gamma_P - 1}\,\frac{\gamma_B + 1}{\gamma_P + 1}\,\frac{\rho_{B_o}}{\rho_{P_o}}} \qquad (25)$$

for the pellet.

Assuming that for the very high pressures and temperatures involved behind the impact shocks, metal exponents are approximately identical, i.e. $\gamma_P = \gamma_B$; these functions have been plotted in Figure 13. It is interesting to note that Equations 24 and 25 permit determination of mean γ's from spray angle envelope measurements (assuming the expansion law is known). It is to be noted that the spray angle is quite sensitive to both polytropic gas exponent and the combination of impacting-bumper materials; a light pellet impacting on a dense bumper (magnesium onto stainless steel) doubles the spray angle for the pellet from the reverse condition (copper pellet onto an aluminum bumper).

It may be observed that the values yielded by Equations 23 and 24 appear to be high when compared to existing experimental data from hypersonic range firings, even assuming the large values of γ. Two comments may be made here, first the simple theory advanced here does not account for vaporization energy and condensation effects on undergoing the sudden type expansion associated with the centered wave. In the second instance, experimental results to date have been at too low velocity to provide any cross checking; impact energies were not sufficiently high to meet the assumptions inherent in this simple model, i.e. vaporization energy/shock enthalpy much smaller than unity.

Assuming cylindrical flow, (such as would predominate in Region 3 of Figure 9(b)) the equations to be solved are:

$$\frac{\partial \rho}{\partial t} + u\,\frac{\partial \rho}{\partial r} + \rho\,\frac{\partial u}{\partial r} + \frac{\rho u}{r} = 0$$

$$\frac{\partial u}{\partial t} + u\,\frac{\partial u}{\partial r} + \frac{1}{\rho}\,\frac{\partial p}{\partial r} = 0$$

$$\gamma = \gamma(p,T)$$

with boundary conditions those of a centered wave at $r = r_o$, radial flow durations being bounded by the interaction of the rarefactions. These equations along with the appropriate energy relation can be programmed for numerical solution, including with somewhat considerable increase in complexity, detailed analysis of the interaction regimes. If a constant mean value of γ can be assumed over some expansion region, then the

classical self-similar solutions (Sedov 11, Stanyukovich 9) can be applied directly to give radial distribution of velocity, density, and energy.

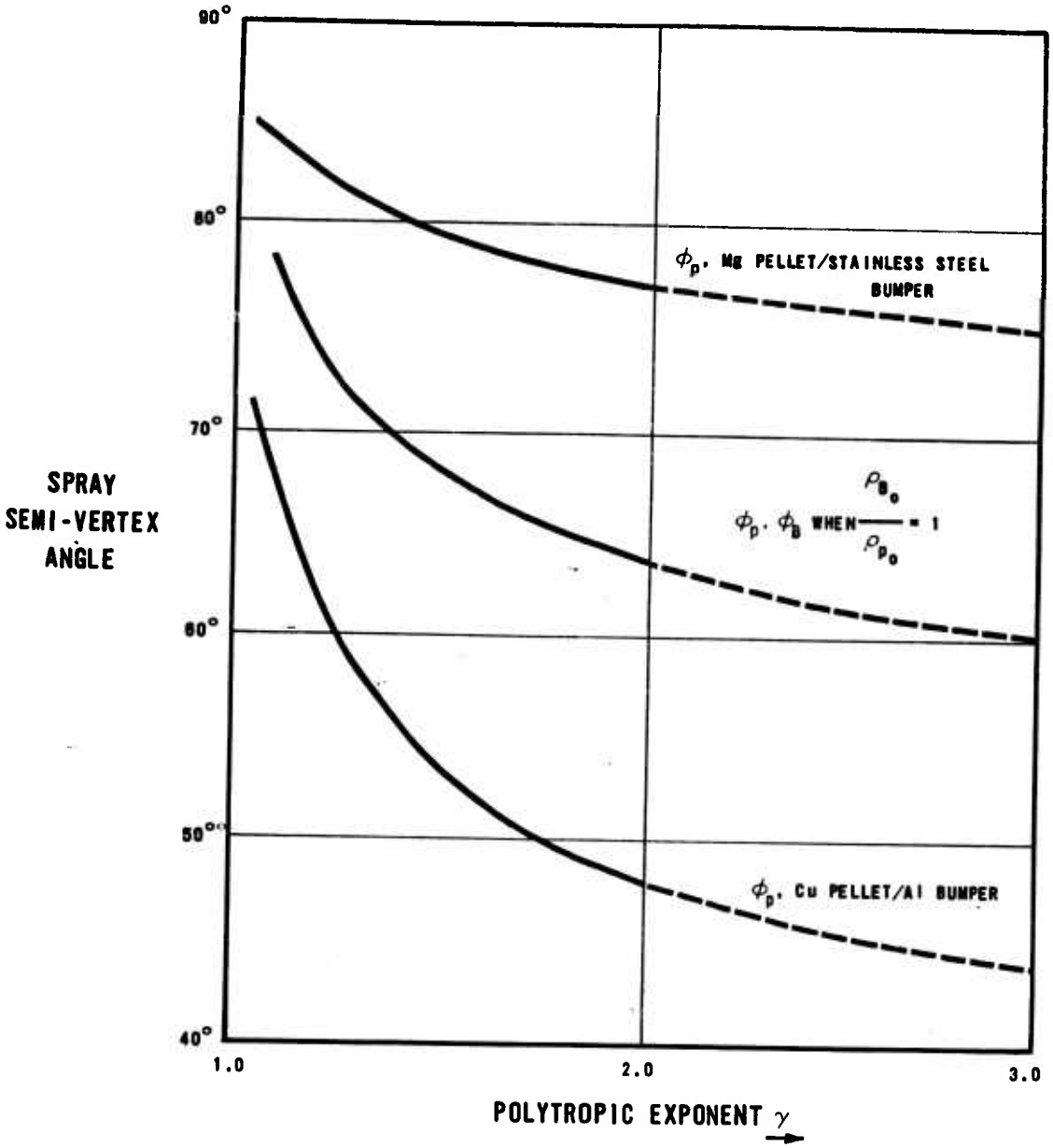

FIGURE 13 Maximum Spray Angles

VIII. DISCUSSION

The present note is intended to summarize some initial thinking on an analytical approach to the break-up of a meteor on impact with a thin flat plate. Periodic extensions and modifications of the approach will be made in light of more extensive work; indeed, even at the time of issuance some of the work has been advanced well beyond the stages described herein. However, it is felt worthwhile to circulate the present write-up, since it does contain considerable detail that will not be repeated in future publications.

In this analysis three main phases of the problem have been discussed, some in considerably more depth than others. One is naturally led to wonder in summary, the states of each phase.

In relation to the first phase, the predictions of pressure and temperature in the impact shock states would appear to be satisfactory as a first approximation, barring, of course, significant electron stripping effects. The comparison with Bjork's computed curve indicates some quite reasonable agreement with more exact computations. These observations are all based on the use of the condensed media $\gamma = 3$. No comparison can be made with any experimental or predicted temperature effects; the Los Alamos work considered only the solid state propagation of shocks and falls well below the applicability of this theory. Electron stripping will lower the temperature and raise the pressure, and this is presently being included in estimation of the impact states.

In relation to the second phase, considerably more effort must be expended on determining the radiant energy flux and its effect on the shock induced and expansion states. Crude estimates would indicate radiative losses throughout the spectrum in the 10^{3} to 10^{4} watts per square centimeter range. These may be expected to lower appreciably the thermodynamic state at which expansion takes place as well as introducing departures from local thermodynamic equilibrium. This phase is perhaps in the least satisfactory condition of all.

Given the thermodynamic states, the expansion flow characteristics can be computed readily. Simple boundary controlled conditions have been presented in this note, and the more detailed solutions to the expansion flows will be presented in another note soon to be published. The more complex problem of expansion from the condensed state (with a $\gamma = \gamma(p,T)$) remains.

Experimentally, shocks have been propagated through columns of gas, and the diffraction and outflow characteristics observed. These studies tend to establish the validity of the basic model and provide some checks, crude though they may be, on the boundary flows. Future experimental work will include the measurement of impact radiation and spray characteristics in the McGill hypersonic firing range.

BIBLIOGRAPHY

1. Proceedings of the Third Symposium on Hyperve

2. Proceedings of the Fourth Symposium on Hyperve

3. Bjork, R. L.; Effects of Meteoroid Impact on
Space: The Rand Corporation; p. 1662, Decembe

4. Stanyukovich, K. P.; Unsteady Motion of Conti
Press, 1961.

5. Walsh, J. M., Christian, R. H.; Equation of S
urements; Physical Review: Volume 97, No. 6,

6. Walsh et al.: Shock-Wave Compression of Twenty
of State of Metals: Physical Review, Volume 1

7. McQueen, R. G. and Marsh, S. P.; Equation of
lic Elements from Shock-Wave Measurements to
Volume 31, No. 7, July 1960.

8. Courant and Friedrichs: Supersonic Flow and S

9. Kurnosova, L. V. (Editor); Artificial Earth S
Plenum Press; p. 307.

10. Sedov, L. I.; Similarity and Dimensional Meth
Press.

11. Glass, I. I., Heuckroth, L. E., and Molder, S
Overtaking of a Rarefaction Wave by a Shock W
Institute of Aerophysics, University of Toron
Report 1488 (Volume 6).